ORIGINAL ARTICLE

Stability of wide-flange columns in steel moment-resisting frames: evaluation of the Canadian seismic design requirements

Abrar Islam[1] · Ali Imanpour[1]

Abstract

This paper aims to evaluate the seismic stability of wide-flange columns of steel moment-resisting frames (MRFs) with emphasis on the 2019 Canadian steel design standard, answer the question of how adequate the seismic provisions are, and propose improvements to the current provisions. The seismic design provisions for Ductile (Type D) steel MRFs with the focus on the stability requirements are reviewed first. The provisions are then applied to a five-story steel MRF with wide-flange beams and columns. Three column design scenarios are studied, (1) MRF with square columns, (2) MRF with deep columns, and (3) MRF with deep columns designed excluding the special stability design provisions specified for columns. The seismic response of the frames is evaluated using the dynamic analysis method to obtain anticipated seismic demands under the design level hazard. Dynamic analysis results are then used to examine the stability response of interior and exterior first-story columns part of the MRFs. The results suggest that the current limiting web width-to-thickness ratio $h/t_w = 37$ for first-story columns specified in CSA S16 is adequate at an axial load of approximately $0.15AF_y$, and the in-plane and out-of-plane stability checks are necessary for the columns above the first story to achieve stable response under major seismic events. Furthermore, columns with a global slenderness ratio $L_b/r_y = 70$, exceeding the prescribed value of 50, can be utilized as the first-story columns in MRFs. An increased axial load limit of $0.35AF_y$ can be adopted for exterior first-story columns.

Keywords Steel moment-resisting frames · Wide-flange columns · Seismic design provisions · Numerical simulation · Seismic response

1 Introduction

Steel moment-resisting frames (MRFs) are widely used as the seismic force-resisting system of building structures, particularly in high seismic regions. Ductile MRFs are designed to dissipate seismic input energy through flexural yielding at beam ends and

✉ Ali Imanpour
  imanpour@ualberta.ca

[1] Department of Civil and Environmental Engineering, University of Alberta, Edmonton, Canada

column bases, and limited shear yielding in the beam-to-column web panel zone joint. MRFs are designed to resist gravity plus seismic load effects and satisfy code-specified story drift limits, which often dictates the selection of beams and columns. Columns of steel MRFs are commonly made of wide-flange members and are designed to resist the combined effect of gravity and seismic loads. According to the modern design standards such as the Canadian steel design standard CSA S16 (CSA 2019), U.S. Seismic Provisions AISC 341 (AISC 2016a, b) and Eurocode 8 (2003), columns, except the ones in the first story, should be designed to remain essentially elastic to ensure achievement of desirable yielding hierarchy in the frame. The first-story columns, however, should be designed such that they possess sufficient strength when the beams respond in the inelastic range and remain stable under code-specified seismic and gravity loads. Additionally, their flexural stiffness should be sufficient to limit the story drift to the drift limit prescribed by the respective building code.

Extensive research studies have been performed in the past to evaluate the inelastic cyclic response of steel MRF columns and beam-to-column moment connections (Popov and Chandramouli 1975; MacRae 1990; Nakashima et al. 1990; Popov et al. 1998; FEMA 355D 2000b; Yu et al. 2000; Shen et al. 2002; Ricles et al. 2004), which led to the development and improvement of the seismic design provisions for steel MRFs in North America. Over the past 2 decades, there has been considerable research into the cyclic behavior of wide-flange columns. Newell and Uang (2008) examined the cyclic inelastic response of steel wide-flange columns with low width-to-thickness ratio and nearly square shape under varying axial loads and large lateral displacements. It was confirmed that columns under high axial force demands can exhibit a stable response and significant rotational capacity with minor flexural strength degradation and twisting. The cyclic stability of deep wide-flange MRF columns was evaluated using large-scale laboratory testing (Ozkula et al. 2017a, b, 2021; Uang et al. 2019; Elkady and Lignos 2014, 2017, 2018a; Cravero et al. 2020). The specimens representing a first-story column were tested under unidirectional and bidirectional loading protocols with various end conditions. The results showed that flexural capacity of wide-flange columns, particularly at large story drifts, is often controlled by local buckling at the end plastic hinge locations. Member stability, including weak-axis flexural buckling or lateral-torsional buckling, was also observed after local buckling in wide-flange columns with high member slenderness ratios, e.g., $L/r_y = 161$. Moreover, it was confirmed that column instability highly depends on its end conditions and is less severe when a fixed-flexible end condition is employed.

The Canadian steel design standard specifies a set of seismic design requirements for columns in Ductile (Type D) and Moderately Ductile (Type MD) MRFs. These provisions consist of the column strength verification using the strong column-weak beam concept at every joint, column in-plane and lateral-torsional stability check for all the columns except the first-story column, and special provisions for first-story columns with base plastic hinging. In lieu of the stability verification for the first-story columns with base plastic hinges, the Canadian steel design standard sets out special requirements by imposing limits on section width-to-thickness ratios, global slenderness ratio and axial load ratio to ensure stable and ductile response under major seismic events. The present work aims to evaluate seismic stability of wide-flange steel columns of Ductile MRFs with emphasis on the stability requirements prescribed by the Canadian steel design standard and propose improvements to the stability design requirements of wide-flange columns in MRFs. A combination of the concentrated plasticity-based numerical model of the MRF and continuum-based finite element model (CFEM) of the interior and exterior first-story columns are used to achieve these objectives. Special attention is given to the development of the seismic demands for

the continuum-based finite element column model through the nonlinear response history analysis (NLRHA).

A review of the Canadian seismic design provisions for steel columns of Ductile MRFs is first provided. A prototype Ductile MRF that features three design scenarios with wide-flange columns: (1) square columns with $d/b_f \approx 1.0$, where d and b_f are the depth and width of the cross-section, respectively, designed in accordance with the current CSA S16 provisions, (2) deep columns with $d/b_f \approx 1.9$ designed in accordance with the current CSA S16 provisions, and (3) deep columns with $d/b_f \approx 1.9$ designed excluding the special stability design provisions specified for MRF columns. The key seismic design parameters including story drifts, column bending, axial force and base rotations are evaluated using the results of the NLRHA. In particular, the moment distribution factor used to verify column stability is examined, and an enhanced design value is proposed. The inelastic cyclic stability response of interior and exterior columns isolated from the MRFs selected are assessed using the CFEM. The results of these analyses are finally used to verify the adequacy of the limiting width-to-thickness ratio for the web, member slenderness ratio and axial load limits, and propose improvements to these requirements.

2 Canadian seismic provisions for columns of ductile MRFs

The key seismic design provisions of the 2019 Canadian steel design standard for ductile MRFs are presented here. Beams shall meet the most stringent width-to-thickness limits specified for Class 1 (i.e., highly ductile sections) that are 7.3 and 58.8 for the flange and web, respectively. The columns are selected from Class 1 or Class 2 sections and their strength is verified when beams reach their probable flexural resistance (i.e., plastic hinging forms at the beam ends) by ensuring the combined flexural capacity of the column sections above and below the joint exceeds the summation of the flexural demands imposed by adjoining beams, i.e., the strong column-weak beam ratio check.

The columns that are expected to remain elastic under seismic loads (e.g., columns other than those in Story 1) should be verified for in-plane and out-of-plane stability using the axial force–bending interaction equation as follows:

$$\frac{C_f}{C_r} + \frac{0.85 U_{1x} M_{fx}}{M_{rx}} \leq 1.0 \tag{1}$$

where C_f and M_{fx} are the factored strong-axis bending moment and axial load, respectively, when the beams reach their respective probable flexural resistance. C_r is the factored axial resistance based on strong-axis buckling mode when verifying in-plane buckling limit state, while the weak-axis buckling resistance is used when the lateral-torsional buckling limit state is examined. M_{rx} is the strong-axis moment resistance computed considering full yielding of the cross-section when in-plane stability is verified and the lateral-torsional buckling resistance when the out-of-plane stability limit state is evaluated. The factor U_{1x} accounts for moment gradient and member level second-order effects, taken as 1.0 for MRFs (Imanpour et al. 2016).

Although stability limit states need not be verified for the first-story column, since the same column profile is often used for the first and second stories, member stability in the second-story columns may control the selection of the column section in the first story.

Special requirements are specified by CSA S16 for the first-story columns with anticipated base plastic hinging to ensure stable and ductile response under major seismic events.

These columns shall comply with the width-to-thickness limits of Class 1 sections. In lieu of the out-of-plane stability check using Eq. 1, which is designed to verify the stability of elastic members, the following lateral bracing requirement shall be met:

$$\frac{L_b}{r_y} \leq \frac{17250 + 15500\kappa}{F_y} \tag{2}$$

in which L_b/r_y is the global slenderness ratio of the member about its weak-axis, L_b represents the unsupported length (e.g., story height) and r_y is the radius of gyration about weak-axis. The factor κ is the ratio of the smaller to the larger factored column end moments, which is positive when the member is in contraflexure (positive for double curvature and negative for single curvature). This factor represents the distribution of bending moment along the length of the member and leads to a more liberal lateral bracing limit when it is positive. When verifying Eq. 2, $\kappa=0$ is recommended unless another value can be justified by a rational analysis. CSA S16 also requires that the factored axial load of the column be limited to $0.30AF_y$ for MRFs located in high seismic regions (Seismic Category 4). This limit is intended to avoid the rapid degradation of the flexural strength of the member under high axial load, which can limit column ductility under seismic loading. For the first-story columns subjected to a factored axial load greater than or equal to $0.15AF_y$, a more stringent limit for the web width-to-thickness ratio h/t_w compared to that of Class 1 sections must be met:

$$\frac{h}{t_w} \leq \frac{700}{\sqrt{F_y}} \quad \text{when } C_f \geq 0.15AF_y \tag{3}$$

where h and t_w are the web clear depth and thickness. When imposing Eqs. 2 and 3 to a wide-flange column using $F_y=350$ MPa as required by CSA S16 for the width-to-thickness check, the global slenderness ratio would be limited to 50, assuming $\kappa=0$, and the h/t_w limit would be 37, eliminating the majority of deep wide-flange sections in design, which would be otherwise ideal to meet the stringent code story drift limits. It is important to note that Eqs. 1 and 3 have been specified for the first time in the 2019 edition of the standard. When flexural yielding is expected at the base of the first-story column, the verification of member stability using the axial force–bending interaction equation is not required, which may only be applicable to square wide-flange members where the potential for lateral instability is unlikely, as confirmed by the results of past experimental and numerical studies (FEMA 2000a, b; Newell and Uang 2008).

3 Loading and Member Design

A five-story office building located in Vancouver, British Columbia, Canada on a class C site was selected in this study. The building measures 63×45 m in the plan as shown in Fig. 1a with an equal beam span (=9.0 m) in both principal directions (seven bays in the longer direction and five bays in the shorter direction). The height of the first story is 4.3 m, and the upper stories are 4.0 m-tall. Continuous columns are used over the first and second stories, with a splice at Story 3 joining the lower story columns to columns covering the rest of the building height. The lateral load-resisting system consists of Type D steel MRFs located on the perimeters in both orthogonal directions. The corner columns
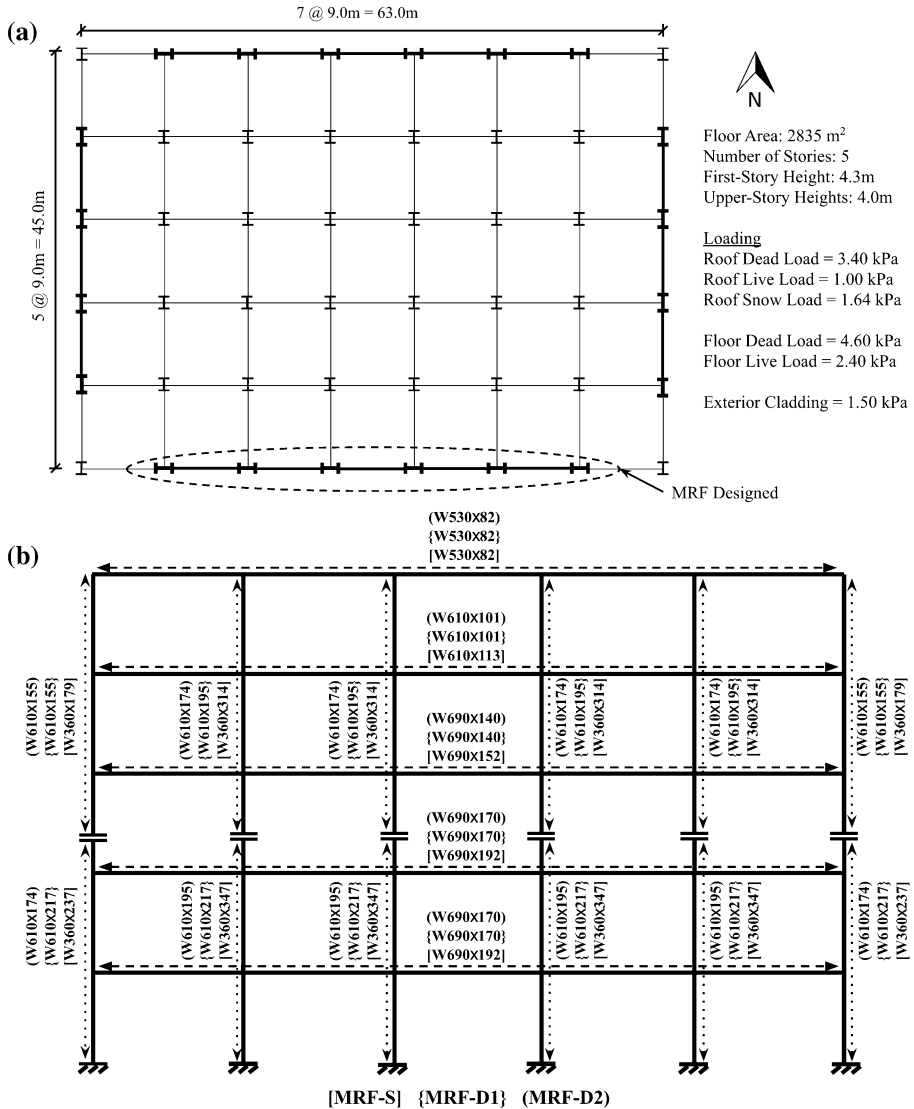
Fig. 1 **a** Plan view of the five-story office building selected; **b** MRF elevation and selected member sizes

and those between the perimeter frames only carry gravity loads. One of the perimeter MRFs in the longer direction was selected and designed in this study.

Loading was performed in accordance with the 2015 National Building Code (NBC 2015) of Canada. The live, dead, and snow load data is provided in Fig. 1a. The seismic load for the preliminary design was calculated using the equivalent static force procedure. The overstrength and ductility-related modification factors R_o and R_d are equal to 1.5 and 5.0, respectively. The selected building is of Normal importance with the seismic importance factor $I_E = 1.0$. The higher mode factor M_v is taken as 1.0. The design period, i.e., the minimum of the fundamental period obtained from a modal analysis and 1.5 times the

period computed using the empirical equation, is $T_a = 1.22$ s, resulting in a design spectral acceleration 0.388 g. The seismic weight tributary to the selected MRF is $W = 31\ 588$ kN.

The selected MRF was designed in accordance with the 2019 edition of CSA S16. Beams and columns were selected from wide-flange (W-shape) sections conforming to ASTM A992 Gr. 50 steel with a nominal F_y and expected $R_y F_y$ yield strength of 345 and 385 MPa, respectively. Three MRF design scenarios were examined, including (1) MRF consisting of square columns with $d/b_f \approx 1.0$ (MRF-S); (2) MRF consisting of deep columns with $d/b_f \approx 1.9$ designed to the current CSA S16 requirements (MRF-D1); and (3) MRF consisting of deep columns $d/b_f \approx 1.9$ designed to the current S16 requirements excluding the special stability design provisions specified for columns in Eqs. 1–3 (MRF-D2). Deep columns are preferred in design because they can efficiently satisfy story drift limits with a lower steel tonnage compared to square sections because of their higher moment of inertia for a given weight. Furthermore, deep sections provide a larger plastic moment capacity, making it possible to more easily meet the strong column-weak beam check at the joints.

Reduced beam section (RBS) connections with circular radius cuts were adopted to ensure beam flexural plastic hinging occurs away from the face of the column. RBS connections were designed and detailed in accordance with CISC Moment Connections for Seismic Applications (CISC 2014). The same beam section is selected for all the bays in each story (Fig. 1b). Maximum allowable flange cuts corresponding to 50% of the flange width were used for the RBS sections at the middle of the reduced area. This is preferred when drift limits govern beam sizes, as is often the case in steel MRFs.

The initial member design was performed using the equivalent static force procedure. The selected members were then used to construct an elastic numerical model of the frame in SAP2000 (CSI 2019). The lateral displacement of the frame at each story was calculated using the model and used to adjust the member sizes so that the NBC story drift limit of 2.5% is met. In the model, gross cross-sections were assigned for the beams; however, the relative lateral displacements obtained from the model was amplified by a factor of 1.1 to account for the stiffness reduction in the beams due to RBS connections (CISC 2014). Once the preliminary sections were selected, a response spectrum analysis was performed and used to choose the final cross-sections for beams and columns. Within each design iteration, the strong column-weak beam ratio was verified at every joint. For MRF-S and MRF-D1 the stability of columns except the first-story columns were verified using Eq. 1. The final sections for the three design scenarios are presented in Fig. 1b. As shown, W360 sections were selected for the columns of MRF-S, while the other two frames consist of deep W610 column sections. Both MRF-D1 and MRF-D2 have the same beam sizes; however, heavier beams were used for MRF-S to increase the frame lateral stiffness in the presence of relatively flexible square W360 columns. The period of the first mode of vibration for MRFs-S, D1 and D2 is 1.87, 1.77 and 1.81 s, respectively. The comparison of steel tonnage between MRFs shows over 20% reduction in steel tonnage when deep columns are used. MRF-D2 was found to be 5% lighter than MRF-D1 because of the relaxation offered when CSA S16 stability requirements are excluded.

For the first-story columns of MRF-D1, κ in Eq. 2 was computed based on the moment distribution corresponding to the condition where the beams reach their full flexural capacity in the RBS region and the plastic moment capacity of the section is developed at first-story column bases. For MRF-D2, the interior column (W610×195) has a web width-to-thickness ratio of 37.2, which is right at the limit as per Eq. 3, and the interaction equation for the lateral-torsional buckling limit state of columns in Story 2 slightly exceeds unity (i.e., 1.04). The web width-to-thickness ratio for the exterior column (W610×174) is 41.0, which exceeds the limit prescribed by Eq. 3. This column is subjected to an axial load of

0.35AF_y, which is above the 0.30AF_y limit. Neither exterior nor interior columns of MRF-D2 satisfy the lateral bracing limit of 50 (i.e., $L_b/r_y = 57$ for W610×195 and $L_b/r_y = 58$ for W610×174).

4 MRF global response

4.1 Concentrated plasticity-based model development

A two-dimensional (2D) nonlinear numerical model of the MRFs shown in Fig. 1b was developed in the *OpenSEES* program (McKenna et al. 1997) to study the global response of the frame using the nonlinear response history analysis (NLRHA) method. The model was constructed using elastic elements (i.e. elasticBeamColumn) simulating the frame stiffness and overall geometry, and nonlinear spring elements (i.e., zero-length) representing flexural plastic hinges at the ends of columns and beams. Beam springs were placed at the center of the RBS while column springs were assigned outside of the beam-to-column web panel zone joint at each story. The properties of zero-length springs are based on the Ibarra Medina Krawinkler (IMK) deterioration model (Lignos and Krawinkler 2011). Nonlinear modeling parameters recommended by Lignos et al. (2019) were used to define the properties of the column springs. The moment capacity of both beams and columns in the spring models were calculated based on the expected yield strength $R_y F_y = 385$ MPa. The modeling technique, as recommended by Zareian and Medina (2010) was used to increase the stiffness of the beam and column rotational springs with a multiplier $n = 10$ (Krawinkler and Ibarra 2005). The strong-axis moment of inertia of beam elements was reduced by 15% to account for the negative effect of the RBS on the lateral stiffness of the frame. This reduction resulted in a 5–10% increase in the lateral displacement of the MRFs under the applied seismic load at each story, which is consistent with the recommendations by FEMA 350 (FEMA 2000a). Beam-to-column web panel zone joints were modeled using the parallelogram model (Gupta and Krawinkler 1999) with rigid elements representing the four boundaries of the panel zone joint and a trilinear rotational spring placed at one of the corners. The horizontal translation of beam-to-column joints at each story was coupled to simulate a rigid diaphragm. The base of MRF columns was modeled as fixed support.

A P-Delta formulation was employed to account for geometric nonlinearities. A leaning column simulated by a truss element with relatively large axial stiffness and pin support at the base was included in the model to reproduce large P-Delta effects due to gravity columns tributary to the MRF. Two ends of the leaning column at each story were simulated as a pin. The leaning column was connected to the MRF at each story using a relatively rigid truss. Lumped masses representing the tributary seismic mass of the frame were equally distributed at the top of columns at each story. To construct the classical damping matrix, the Rayleigh damping approach with mass and stiffness proportional damping corresponding to a critical damping ratio of 2% in the first and second vibration modes was used. Mass proportional damping was assigned to the nodes with point masses, and stiffness proportional term was assigned to elastic elements (Zareian and Medina 2010). Gravity loads tributary to the MRF were applied to the top end of the MRF columns at each story, and the remaining gravity loads were applied to the leaning column at each story. Nonlinear response history analyses were then performed by applying a set of ground motion accelerations in the horizontal direction.
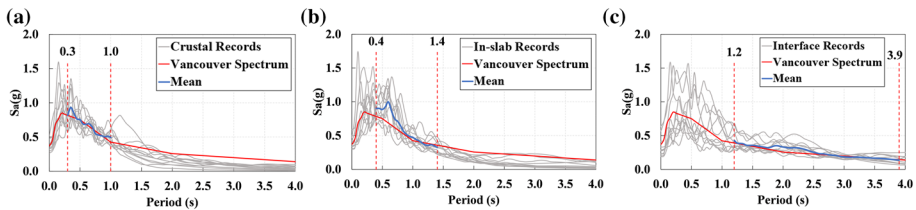
Fig. 2 Response spectra of the selected ground motion records: **a** crustal; **b** deep in-slab; **c** interface subduction

4.2 Ground motion selection and scaling

A suite of 33 earthquake ground motion records consisting of three earthquake scenarios likely in Vancouver, BC, crustal, deep in-slab and interface subduction (11 records per each scenario) was selected and scaled to match on average the NBC design response spectrum of the selected site. This corresponds to a hazard level representing 2% probability of exceedance over 50 years of building life expectancy. The selection and scaling procedures as well as the requirements on the various sources of earthquakes and the number of records follow the recommendations of Commentary J of the NBC (NRC-Commentaries 2015) and those by Tremblay et al. (2015). Response spectra of the scaled records and the average of each suite over their corresponding period ranges for scaling are plotted in Fig. 2 against the NBCC design spectra for Vancouver, site class C. Additional information on the selection and scaling of the records can be found in Ashrafi and Imanpour (2021).

4.3 Global response

The statistics of key seismic response parameters, including the story drift ratio, column axial force and bending moment demands, and column end rotations were calculated for each frame by taking the maximum of means over the earthquake ensembles of the peak response parameter obtained under each ground motion record as recommended by the Commentary J of the NBC (NRC 2015). It is important to recognize that the statistics of the NLRHA are often governed by interface subduction earthquakes for the MRFs studied here.

For all three MRFs studied, the nonlinear response involving plastic hinging at beam ends and the base of the first-story columns was observed for the vast majority of the ground motions. Frame collapse, which is defined as the complete loss of story shear resistance due to P-Delta effects accelerated by component stiffness and strength degradation (Suzuki and Lignos 2020), only occurred for MRF-D2 under the 2011 Tohoku, Japan—YMT002 record. The results associated with this record were discarded as an unacceptable response (NRC-Commentaries 2015), and the response parameters were determined using the results of the remaining records. Figure 3a shows the profiles of story drift ratios for the MRFs studied. As shown, MRF-S exhibits larger drift demands compared to the other two MRFs, which is attributed to lower flexural stiffness contributed by the columns of MRF-S. Moreover, the drift demands at the second and third stories of MRF-S exceed the code-specified limit of 2.5% mainly because of large displacements developed under 5 severe interface subduction records. The lateral displacement of MRF-D1 and MRF-D2 were appreciably lower than MRF-S for the bottom three stories, where the greatest drift
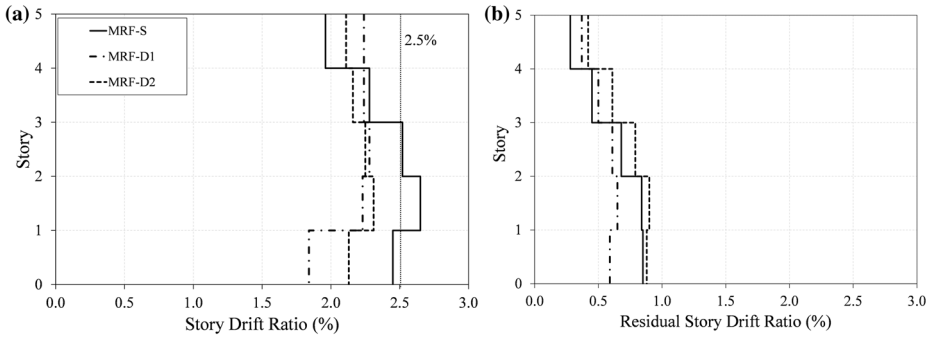
Fig. 3 **a** Profile of peak story drift ratios; **b** profile of residual story drift ratios

demands were observed, with a reduction of 17% and 12%, respectively. This reaffirms the preference in utilizing deep wide-flange column sections to help satisfy the stringent story drift limits prescribed by building codes. The comparison between the story drift ratio in the first story of MRF-D1 and MRF-D2 shows that the former experienced 16% lower drift. The statistics of residual story drift ratios were also computed using the relative lateral displacement of each story at the end of each analysis. The profiles of residual story drift ratios are shown in Fig. 3b. As shown, the residual displacements present in the building following the earthquake events created on average approximately 0.62, 0.54 and 0.72% drift ratio in MRFs-S, D1 and D2, respectively, across all the stories. Moreover, MRF-D2 experienced the largest residual drift ratio, on average about 20% higher than that recorded for MRF-S and 30% higher than that observed for MRF-D1 at each story.

Column flexural bending, axial force and rotation at the member ends were normalized to the probable plastic moment capacity $M_{c,prob}$ given in Eq. 4 (Lignos et al. 2019), axial yielding capacity AF_y, and yield rotation using $n = 10$, respectively.

$$M_{c,prob} = 1.15 Z_x R_y F_y \left(1 - \frac{P_g}{2P_{ye}} \right) \text{ when } \frac{P_g}{P_{ye}} < 0.20 \qquad (4)$$

where P_g and P_{ye} are the column gravity load and the axial capacity computed using the expected yield strength of the material AR_yF_y, respectively. The peak response parameters along with the range of each parameter are given in Table 1 for one of the interior columns and one of the exterior columns in Stories 1–3. It is worth noting that the force and rotation demands for all four interior columns and both exterior columns are nearly identical.

Referring to Table 1, the results of base moment and rotation obtained from the base spring of first-story columns (both interior and exterior) indicate that flexural yielding occurred at their bases. The results of the peak base moment and rotation show that MRF-D2 columns, on average experienced the largest normalized base moments ($1.05M_{c,prob}$) and rotations ($21.2\theta_y$). The maximum value of the base moment reached $1.09M_{c,prob}$ for the interior column of MRF-D2 and the maximum rotation $33.4\theta_y$ was observed at the base of the same interior column. No yielding occurred at the top end of the first-story columns of MRF-S and MRF-D1; however, limited yielding was observed at the top end of the interior columns in MRF-D2 ($\theta_{PH} = 1.5\theta_y$) under the 2001 Southern Peru—POCO record, which could potentially result in the formation of a soft story mechanism. Limited plastic rotations were also observed at the base of the second story for the same interior column of MRF-D2 ($\theta_{PH} = 1.6\theta_y$) under the 2010 Maule-SSA2 record. Furthermore, as global frame

Table 1 Column bending moment, axial force and rotation in Stories 1 – 3

Parameter	MRF-S		MRF-D1		MRF-D2	
	Interior	Exterior	Interior	Exterior	Interior	Exterior
Story 3						
$M_x/M_{c,prob}^{Top}$	0.67 (0.34–0.78)	0.62 (0.32–0.73)	0.70 (0.33–0.83)	0.52 (0.26–0.74)	0.76 (0.39–0.88)	0.53 (0.27–0.79)
$M_x/M_{c,prob}^{Bottom}$	0.69 (0.40–0.85)	0.65 (0.38–0.81)	0.73 (0.39–0.94)	0.55 (0.34–0.77)	0.80 (0.43–0.92)	0.55 (0.34–0.68)
$\theta_{PH}/\theta_y^{Top}$	0.60 (0.40–0.70)	0.60 (0.40–0.70)	0.70 (0.30–0.90)	0.50 (0.30–0.70)	0.70 (0.30–0.90)	0.50 (0.30–0.90)
$\theta_{PH}/\theta_y^{Bottom}$	0.70 (0.40–0.90)	0.60 (0.40–0.80)	0.70 (0.30–0.90)	0.50 (0.30–0.70)	0.90 (0.30–0.90)	0.50 (0.30–0.70)
C_f/AF_y	0.06 (0.06–0.06)	0.18 (0.16–0.18)	0.09 (0.09–0.10)	0.20 (0.19–0.21)	0.10 (0.10–0.10)	0.20 (0.19–0.21)
Story 2						
$M_x/M_{c,prob}^{Top}$	0.74 (0.40–0.82)	0.60 (0.34–0.67)	0.73 (0.46–0.86)	0.45 (0.29–0.61)	0.82 (0.48–0.92)	0.55 (0.32–0.69)
$M_x/M_{c,prob}^{Bottom}$	0.66 (0.31–0.73)	0.53 (0.26–0.61)	0.73 (0.33–0.92)	0.44 (0.21–0.67)	0.80 (0.37–1.00)	0.52 (0.25–0.72)
$\theta_{PH}/\theta_y^{Top}$	0.70 (0.40–0.90)	0.60 (0.40–0.70)	0.70 (0.50–0.90)	0.50 (0.30–0.70)	0.90 (0.50–0.90)	0.50 (0.40–0.70)
$\theta_{PH}/\theta_y^{Bottom}$	0.60 (0.40–0.70)	0.50 (0.20–0.60)	0.70 (0.30–0.90)	0.50 (0.20–0.70)	0.90 (0.40–1.60)	0.50 (0.20–0.70)
C_f/AF_y	0.07 (0.07–0.07)	0.21 (0.16–0.21)	0.12 (0.11–0.12)	0.22 (0.17–0.22)	0.13 (0.12–0.13)	0.27 (0.21–0.28)
Story 1						
$M_x/M_{c,prob}^{Top}$	0.69 (0.50–0.89)	0.59 (0.43–0.80)	0.61 (0.40–0.79)	0.41 (0.27–0.60)	0.75 (0.49–1.00)	0.57 (0.36–0.82)
$M_x/M_{c,prob}^{Bottom}$	1.02 (0.73–1.04)	1.01 (0.69–1.06)	1.04 (0.70–1.08)	1.02 (0.62–1.08)	1.05 (0.76–1.09)	1.04 (0.71–1.08)
$\theta_{PH}/\theta_y^{Top}$	0.70 (0.40–0.90)	0.60 (0.40–0.80)	0.7 (0.30–0.80)	0.30 (0.30–0.70)	0.80 (0.50–1.50)	0.50 (0.30–0.80)
$\theta_{PH}/\theta_y^{Bottom}$	13.0 (0.80–32.6)	11.5 (0.70–30.3)	13.9 (0.70–28.2)	11.4 (0.7–25.3)	21.2 (0.8–33.4)	19.0 (0.70–31.7)
C_f/AF_y	0.09 (0.09–0.09)	0.27 (0.18–0.28)	0.15 (0.14–0.16)	0.28 (0.19–0.29)	0.17 (0.16–0.17)	0.35 (0.23–0.36)

instability occurred under the 2011 Tohoku, Japan-YMT002 record, a flexural plastic hinge formed at the top end of the interior first- and second-story columns. Such instances of limited yielding at locations above the fixed base plastic hinge in MRF-D2 indicate that satisfying only the strong column-weak beam ratio may not be sufficient to ensure elastic response and prevent instability of the columns above the first story.The verification of the in-plane and out-of-plane stability of such columns under the expected loads arising from flexural yielding in the beams are needed (i.e., Eq. 1). For MRF-S and MRF-D1 no yielding was observed in the upper-story columns. The comparison between the flexural response reported for interior and exterior columns in Table 1 shows that exterior columns always experienced plastic rotations, indicating less severe local buckling and flexural strength degradation in such columns compared to their interior counterparts (Lignos et al. 2019). This is expected as the exterior columns are loaded by only a single moment connection as opposed to two for interior columns and experience fluctuating axial loads due to dynamic overturning effects as opposed to a constant gravity load likely in interior columns. As shown in Table 1, the axial loads in the interior first-story columns of MRFs-S, D1 and D2, which were induced by gravity loads only, reached a maximum value of $0.09AF_y$, $0.15AF_y$, $0.17AF_y$, respectively. Higher axial loads were however observed in the exterior columns, namely, $0.27AF_y$ and $0.28AF_y$ in the first story of MRF-S and MRF-D1, respectively, and $0.35AF_y$ in the first story of MRF-D2. The higher axial loads on the exterior columns are attributed to the dynamic overturning effects. The peak axial loads in the first-story columns of MRF-S and MRF-D1 remained below 30% of the nominal axial capacity of the member, which matches well with design requirements, whereas the axial load in the first-story columns of MRF-D2 exceeded this limit.

4.4 Evaluation of the lateral stability requirement

The lateral bracing requirement of Eq. 2 was originally developed for I-shaped beams with flexural plastic hinging based on the experimental test data by Bansal (1971) (Bruneau et al. 2011). Unless a rational analysis is carried out by the designer, CSA S16 requires $\kappa = 0$ for the first-story columns, which represents the moment diagram where the moment reaches nearly zero at the top end of the member while the base yields and develops its full plastic capacity under an earthquake ground motion (Imanpour et al. 2016). The factor κ was computed for the first-story columns of the three MRF designs in this study. Figure 4 shows the variation of κ with respect to the normalized top moment and story drift ratio Δ/L, where Δ is the relative lateral displacement of the story and L is the height of the first-story column, for the interior and exterior columns of MRFs-D1 and D2 under the 2007 Pisco-UNICA record. Since the moment at the column base is expected to reach the probable plastic moment of the section, the top moment is used here as it can represent the moment demand induced in the column under seismic loading. The top moment was calculated at the beam centerline by projecting the moment measured underneath the beam-to-column web panel zone to reproduce the moment typically used in design which is also aligned with the unbraced length of the column assumed in design.

It is apparent from Fig. 4 that κ tends to remain positive (i.e., member in double curvature) and often above 0.2 in particular when the story drift ratio exceeds 2%. $\kappa \leq 0$ (i.e., member in single curvature) was observed only when the column moment demand is minimal (e.g., $< 0.2M_{c,prob}$). The observed trend for MRFs-D1 and D2, as shown in Fig. 4 is similar for all the columns of the three design scenarios under all the ground motions.
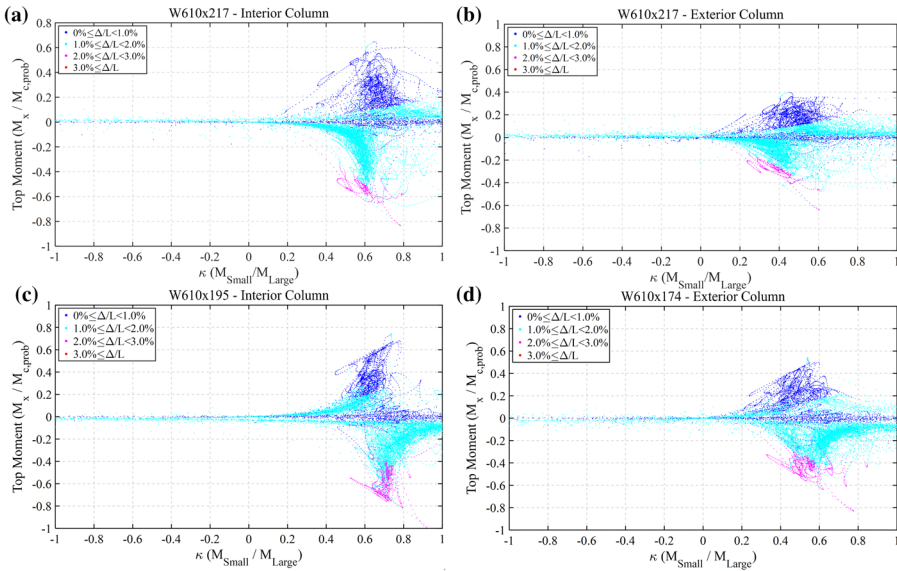
Fig. 4 Variation of κ versus top moment and story drift ratio for the first-story columns (interior and exterior) under the 2007 Pisco-UNICA record: **a** MRF-D1; **b** MRF-D2

Additionally, interior columns always have a higher κ value compared to exterior columns. This is due to lower moment demands induced in exterior columns.

A weighted average $\overline{\kappa}$ was computed using the κ values obtained from the NLRHA for all the first-story columns:

$$\overline{\kappa} = \frac{\sum \kappa \times \Delta/L}{\sum \Delta/L} \tag{5}$$

In this equation, story drift ratio is used as the weighting factor because column out-of-plane instability is unlikely at lower story drift ratios with very limited yielding and local buckling at the column base (Ozkula et al. 2017a, b; Elkady and Lignos 2018a). The statistics of the peak $\overline{\kappa}$ values including the range of variations are presented in Table 2. $\overline{\kappa}$ values vary between 0.26 and 0.77 for interior columns and between 0.11 and 0.64 for exterior columns of MRFs-D1 and D2, suggesting that the value currently prescribed by CSA S16, i.e., $\kappa = 0$, may not well represent the first-story column moment ratio under seismic loading. Using the minimum value of peak $\overline{\kappa}$ from Table 2 that is 0.63 for the interior deep columns and 0.45 for exterior deep columns, and assuming $F_y = 345$ MPa, the lateral bracing limit from Eq. 2 increases to 78 for the interior columns and to 70 for the exterior columns. This would permit the designer to use more slender columns such as W610×217 and W610×174 selected in this study for MRFs-D1 and D2, respectively. Such columns would be unacceptable for use in steel MRFs when applying the current CSA S16 provisions, i.e., the lateral bracing limit of 50. Furthermore, it was found that for both the interior and exterior columns, on average, κ remains positive in nearly 90% of the duration of a ground motion. These results suggest the possibility of relaxing the lateral bracing limit by using a κ value larger than zero in the design of first-story MRF columns.

Table 2 Weighted average $\overline{\kappa}$ for the first-story interior and exterior columns

Design scenario	Location	Section	Mean $\overline{\kappa}$
MRF-S	Interior	W360×347	0.75 (0.33–0.83)
	Exterior	W360×237	0.66 (0.35–0.78)
MRF-D1	Interior	W610×217	0.63 (0.26–0.72)
	Exterior	W610×217	0.45 (0.11–0.58)
MRF-D2	Interior	W610×195	0.68 (0.35–0.77)
	Exterior	W610×174	0.53 (0.29–0.64)

5 First-story column response

5.1 Continuum finite element model development

A three-dimensional continuum finite element model (CFEM) of the first-story column was created in the *Abaqus* finite element program (Simulia 2020) to evaluate the local response of the MRF columns, in particular, verify the adequacy of the CSA S16 stability design requirements and propose potential improvements to these provisions. The CFEM can provide insight into the column local response with explicit consideration of initial geometric imperfections, residual stresses, global and local buckling limit states. An isometric view of the CFEM is shown in Fig. 5a. The column extends from the column base to the beam centerline with a length corresponding to the MRF first story (Fig. 1b). The column was simulated using four-node doubly curved, reduced integration, hour-glass controlled shell elements with a uniform mesh size of 25×25 mm. The adjoining beams at the top end of the column, including the RBS connection and the beam outside of the reduced area, were modeled using beam elements spanning half the beam span length (i.e., 4.5 m on each side of the column centerline for the interior column and 4.5 m on one side of the column centerline for the exterior column). These beams were intended to represent the strength and stiffness of the adjoining first-story beams assuming an inflection point at the beam mid-span under the lateral seismic load. The RBS region was partitioned into five sections, with the flange width adjusted along the RBS length to represent the reduced flange region. Material nonlinearity was incorporated in the model through the Maxwell-Huber-Hencky-von Mises yield criterion with associated flow rule. The nonlinear cyclic behavior of the steel material was reproduced using the Voce and Chaboche plasticity model that features combined isotropic/kinematic hardening (de Castro e Sousa et al. 2020; Hartloper et al. 2021). The material was defined using Young's modulus, $E = 200$ GPa, Poisson's ratio $\upsilon = 0.3$, and the expected yield stress $R_yF_y = 385$ MPa. The steel stress–strain cyclic inelastic behavior is defined with one backstress using kinematic hardening parameters, including the kinematic hardening modulus $C = 3378$ MPa and rate at which the kinematic hardening modulus decreases with increasing plastic deformation $\gamma = 20$, and the isotropic hardening parameters, including the maximum change in the size of the yield surface $Q_\infty = 90$ MPa and the rate at which the size of the yield surface changes as plastic straining develops $b = 12$ (Elkady and Lignos 2018b). The residual stress distributions proposed by Galambos and Ketter (1958) in which a linear distribution is assumed in the flange and uniform tension stress is assigned to the web, were considered as shown in Fig. 5b. An elastic-perfectly plastic material model with the expected yield stress was assigned to the
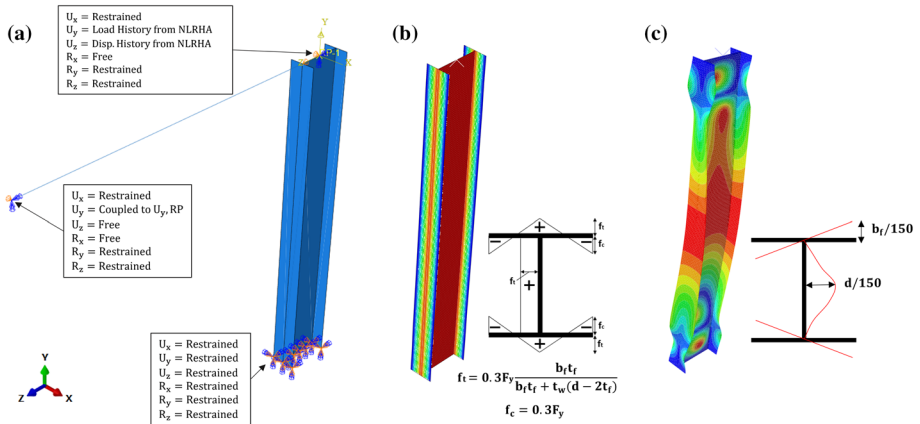
Fig. 5 Continuum finite element model: **a** boundary conditions (exterior column shown); **b** residual stress distributions; **c** local plus global initial geometric imperfections

elements creating the RBS while the rest of the member outside of the reduced region was simulated using an elastic material.

To trigger local and global buckling in the column, initial geometric imperfections were introduced as shown in Fig. 5c. Local imperfections were created in the web and flanges at both ends of the column to reproduce anticipated manufacturing errors (ASTM 2003) with maximum amplitudes of $b_f/150$ and $d/150$ in the flange and web, respectively. The global out-of-straightness, which is affine to the global buckling mode of the column about its weak-axis, was created in the model with a maximum amplitude of 1/1000 times the member unsupported length (AISC 2016a, b).

Figure 5a shows the boundary conditions of the CFEM. At the column base, both the translational and rotational degrees-of-the-freedom (DOFs) were restrained. At the top end of the column, the translation and rotation of the column nodes were coupled to a reference point (RP in Fig. 5a) at the middle of the column web. The out-of-plane translation at the RP was restrained, representing the lateral support provided by perpendicular beams framing into the column at the story level. The other two translational DOFs, including axial displacement along Y-axis and lateral displacement along Z-axis were controlled by the axial load and displacement histories obtained from the NLRHA performed in the *Open-SEES*. The rotation about X-axis was released as it is explicitly reproduced using the first-story beams while the rotations about the other two axes were restrained to represent the flexural, torsional and warping stiffness offered by upper-story columns not simulated here. The translational and rotational DOFs of the beam end were tied to those of the top end of the column to simulate the beam rigid connection. At the far end of the beams, the longitudinal movement along Z-axis and rotation about X-axis were released while the translation along X-axis and rotations about Z- and Y-axes were restrained. The vertical translation along Y-axis was set equal to the longitudinal displacement of the top end of the column. The groove welds between the beam flange and column flange as well as the beam web connection plates, were not explicitly simulated in the CFEM. Furthermore, the beneficial effects of the concrete slab on providing the lateral support to the beams were ignored since concrete may not be effective after cracking at large story drift ratios (Ricles et al.
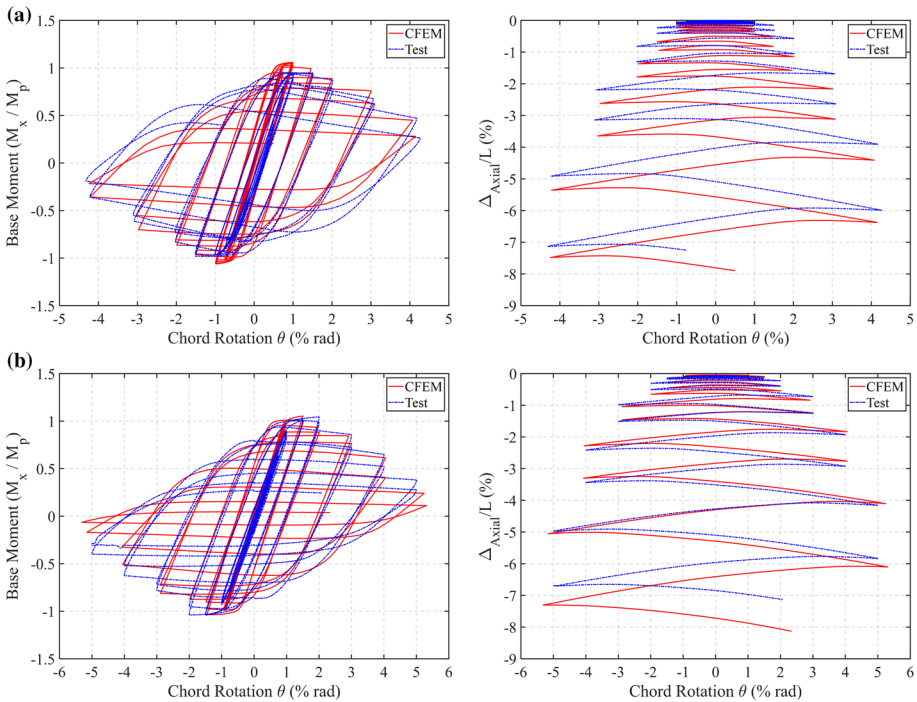
Fig. 6 CFEM validation for: **a** W610×217 specimen with fixed–fixed end condition; **b** W610×217 specimen with fixed–flexible end condition

2004; Zhang and Ricles 2006), which is expected under major earthquake events. Geometric nonlinearity was considered through large-displacement formulations.

The CFEM was validated using the experimental test data of wide-flange MRF columns by Elkady and Lignos (2018a). For the validation study, two column specimens consisting of W610×217 section and two end conditions consisting of fixed–fixed and fixed-flexible were considered. Identical modeling assumptions as those described for the CFEM were used to develop the numerical model of the selected experimental specimens except that the first-story beams of Fig. 5a were removed in the calibration model. Figure 6a, b show base moment—chord rotation and axial shortening—chord rotation responses obtained from the CFEM developed here as compared to those of the physical test data for the fixed–fixed and fixed-flexible specimens, respectively. In this figure, M_p is the plastic moment capacity about the section major axis based on measured material and geometric properties, and L is the height of the column specimen.

The comparisons shown in Fig. 6a, b confirm that the CFEM can appropriately reproduce the cyclic inelastic behavior of wide-flange steel columns, including flexural strength and stiffness degradations due to flange and web local buckling as well as lateral out-of-plane deformations. The slight overestimation of the specimen moment capacity by the CFEM (Fig. 6a) can be attributed to the minor flexibility of the testing equipment (Imanpour 2015), which affected more the response of a fixed–fixed column specimen compared to the fixed-flexible case. The overestimation of the extent of axial shortening in both fixed–fixed and fixed-flexible cases can stem from a more critical initial imperfection

amplitude used, which is likely higher than the actual initial imperfection amplitude of the specimens (Elkady and Lignos 2018b), e.g., because of advanced fabrication practice.

5.2 Cyclic response

The interior and exterior first-story columns of the three design scenarios (MRFs-S, D1 and D2) studied were analyzed using the CFEM developed here under the time history of the in-plane displacement along the Z-axis, creating strong-axis bending and the time history of the axial load along Y-axis. The displacement and load histories were obtained from the NLRHA performed using the concentrated plasticity-based model in *OpenSEES* and were applied at the top end of the CFEM. For each design scenario (see Table 3), the record associated with each of the three earthquake ground motion suites (crustal, deep in-slab, interface) that yielded the largest story drift ratio in the first story of MRF-D2 was selected to perform the analyses and examine the design limits. The selected records were 1992 Landers—Desert Hot Springs, 1949 Olympia—Highway Test Lab and 2011 Tohoku, Japan—YMT002 for crustal, deep in-slab and interface subduction earthquakes, respectively. Among these records, the subduction interface event always produced the largest drift demands on the column compared to the other two scenarios. For MRF-D2, the 2011 Tohoku record resulted in frame instability at 150 s; thus, the analysis was only completed for the portion of the record until a chord rotation of 6.5% was reached. The applied axial load history obtained from the selected response history analysis was relatively constant for the interior columns; however, the exterior columns were subjected to varying axial loads due to overturning effects.

Figure 7 shows the normalized base and top moments versus the respective chord rotations for the interior MRF columns under 2011 Tohoku, Japan—YMT002 record. The W360×347 column of MRF-S exhibited a stable response with significant strain hardening without any noticeable strength degradation or local buckling despite a relatively high drift demand of 4.3%. The column experienced minimal flange local buckling at its base at the end of the analysis, as shown in Fig. 7a. The flexural strength of the W610×217 column of MRF-D1 at its base reached $1.15R_yM_p$ prior to degradation at 2.8% chord rotation ($1.09R_yM_p$) due to flange and web local buckling, which is initiated at 2.0% chord rotation but exacerbated at higher drift demands. Both W360×347 and W610×217 columns experienced minor axial shortening at the end of the ground motion with an amplitude of $0.16\%L$ and $0.24\%L$, respectively. Limited yielding without local buckling was observed at the top end of these two columns.

The W610×195 column selected for MRF-D2, which is the most slender member between the interior columns of the three MRFs studied here and has a web width-to-thickness ratio close to the CSA S16 limit, experienced significant local buckling combined with limited out-of-plane deformation at the base plastic hinge, which led to significant strength degradation compared to the interior column of the other two designs. The moment capacity at the base was reduced to $0.89R_yM_p$ at 4.0% chord rotation, which is above the threshold of $0.80R_yM_p$ typically used as the performance measure for beam-to-column moment connections (AISC 2016a, b), and to $0.84R_yM_p$ at 6.5% rotation precipitated by severe local buckling and out-of-plane deformation at the base. Additionally, local buckling and significant strength degradation occurred at the top end of the column, confirming the soft story mechanism observed in the NLRHA. The W610×195 column was subjected to higher axial load demands compared to the other interior columns with a maximum value of $0.17AF_y$, which combined with limited out-of-plane deformation at the

Table 3 Cross-sectional properties and force capacities for the first-story columns

Design scenario	Location	Section	L_b/r_y	$b_f/2t_f$	h/t_w	I_x (mm⁴)	C_w (mm⁶)	J (mm⁴)	$AR_yF_y^a$ (kN)	$R_yM_p^a$ (kNm)
MRF-S	Interior	W360×347	41.3	4.6	11.7	1.3E+09	1.6E+13	2.5E+07	17,017	2749
	Exterior	W360×237	42.2	6.6	17.0	7.9E+08	9.6E+12	8.2E+06	11,589	1810
MRF-D1	Interior	W610×217	56.2	5.9	34.6	1.9E+09	1.5E+13	5.6E+06	10,665	2637
	Exterior	W610×217	56.2	5.9	34.6	1.9E+09	1.5E+13	5.6E+06	10,665	2637
MRF-D2	Interior	W610×195	57.0	6.7	37.2	1.7E+09	1.3E+13	4.0E+06	9587	2333
	Exterior	W610×174	57.6	7.5	41.0	1.5E+09	1.1E+13	2.8E+06	8547	2064

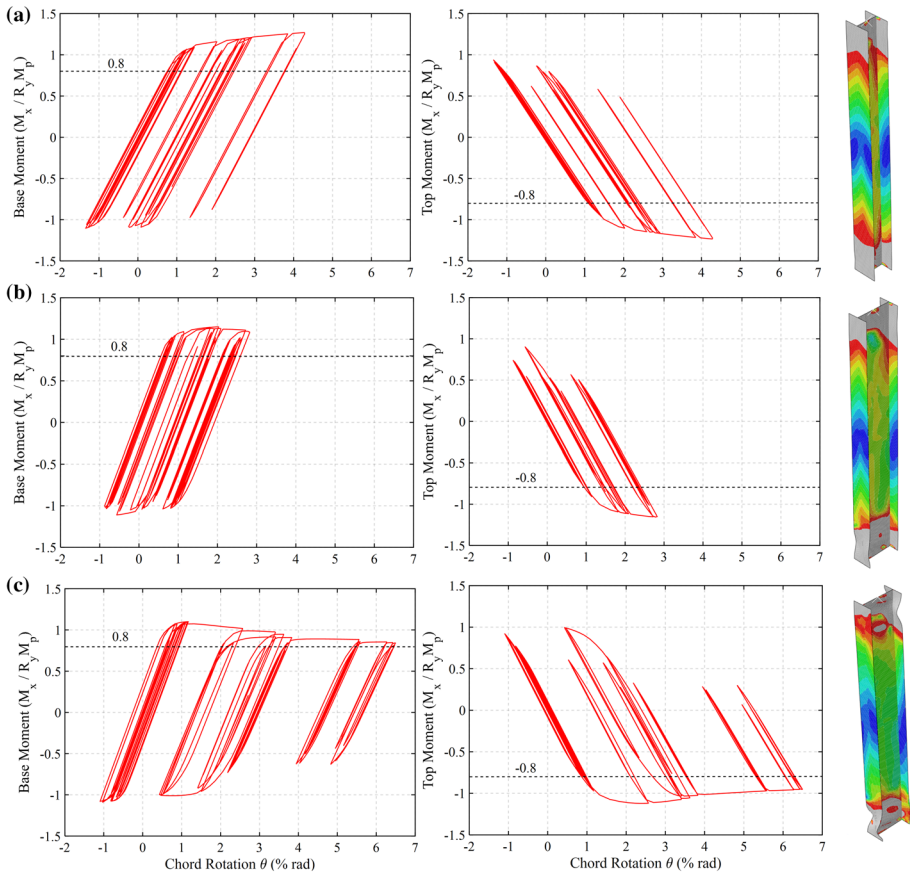[a] Strength based on expected yield stress of R_yF_y =385 MPa

Fig. 7 Moment-chord rotation response and deformed-shape corresponding to maximum chord rotation for the interior first-story columns under the 2011 Tohoku—YMT002 earthquake: **a** W360×347 of MRF-S1; **b** W610×217 of MRF-D1; **c** W610×195 of MRF-D2 (gray area represents yielding regions)

base plastic hinge, and flange and web local buckling initiated at 1.6% chord rotation at the base, resulted in an axial shortening of 1.1%L at the end of the analysis. This axial shortening is approximately four times more than the axial shortening observed for the other two interior columns.

The moment responses of the exterior columns subjected to the 2011 Tohoku, Japan—YMT002 record are shown in Fig. 8. The W360×237 column of MRF-S and W610×217 of MRF-D1 exhibit significant strain hardening without noticeable flexural strength degradation. Limited flange local buckling was observed only at the base of these columns (Fig. 8a, b). The maximum axial shortening reached 0.09%L and 0.08%L for W360×237 and W610×217, respectively. The W610×174 column of MRF-D2, however exhibited more pronounced local buckling in the web and flanges. Local instability at the base plastic hinge reduced the moment capacity of the column to 0.97$R_y M_p$ at 6.5% rotation. The maximum axial shortening recorded at the end of the analysis was equal to 0.6%L, which is nearly six times that of W360×237 and W610×217 columns. The W610×174 column has a web slenderness ratio of 41.0 and experienced a
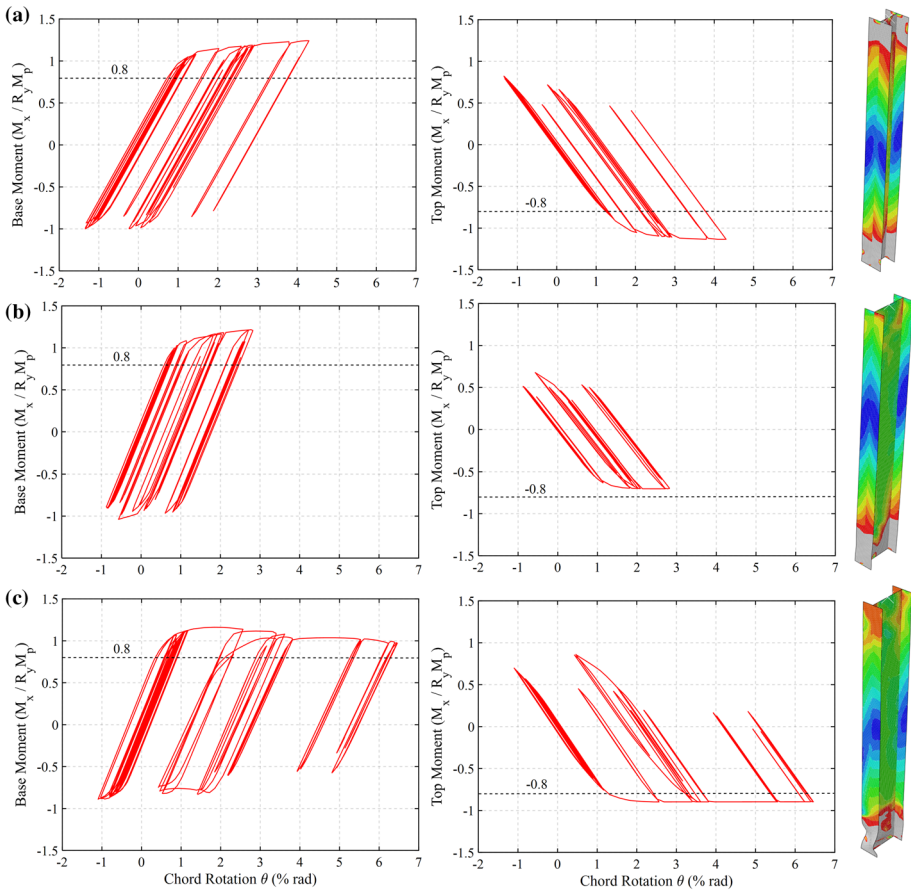
Fig. 8 Moment-chord rotation response and deformed-shape corresponding to maximum chord rotation for exterior first-story columns under the 2011 Tohoku—YMT002 earthquake: **a** W360×237 of MRF-S1; **b** W610×217 of MRF-D1; **c** W610×174 of MRF-D2 (gray area represents yielding region)

maximum axial load of $0.35AF_y$; both values are above the code-specified limits for columns with anticipated base plastic hinging. Exterior columns, on average, experienced lower strength degradation compared to interior columns, which are under higher gravity-induced axial loads.

The responses of the interior and exterior columns under the crustal and deep in-slab ground motion records followed the trend observed under the subduction interface record with the column sections of MRF-D2 showing the most severe local instability and greatest strength degradation, although no collapse was recorded under the crustal and deep in-slab records. Moment and drift demands under the crustal and deep in-slab records were always lesser than those from the interface ground motions. For instance, story drift ratios remained below 2.5%, and the moment capacity of the first-story columns did not fall below $1.0R_yM_p$. It is worth noting that the stable responses observed for the W360 sections of MRF-S align well with past experimental studies (Newell and Uang 2008).

The results of the CFEM analyses showed no member instability or excessive out-of-plane deformations for the deep interior and exterior columns of MRF-D1, which both
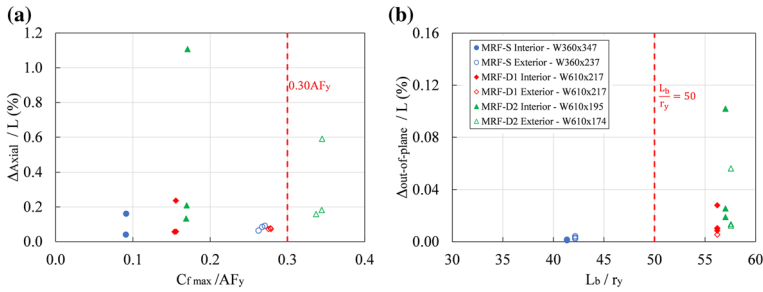
Fig. 9 **a** Normalized axial shortening versus compressive axial load ratio; **b** normalized out-of-plane deformation along the member length

violate the lateral bracing limit of 50 assuming $\kappa = 0$ (see Eq. 2). As such, this lateral bracing requirement is deemed conservative. This observation is further reinforced by the findings of the NLRHA for the κ factor described earlier. Moreover, the comparison between the results of MRF-D1 and MRF-D2 columns shows the necessity of stability requirements such as Eqs. 1 and 3 for MRF columns with base plastic hinging. Had such stability requirements been neglected in the design of MRF-D1 columns, the instability mode similar to that observed under the 2011 Tohoku, Japan—YMT002 record would have been expected, which could have led to frame collapse.

5.3 Influence of axial load

Column axial shortening was used to evaluate the compressive axial load limit for the first-story columns. For the columns studied here, the record associated with each of the three earthquake ground motion suites (crustal, deep in-slab, subduction interface) that yielded the largest story drift ratio in the first story of MRF-D2 was used. The maximum normalized axial shortening Δ_{axial}/L under each ground motion record is plotted against the maximum value of the normalized compressive axial load $C_{f,max}/AF_y$ under the same record in Fig. 9a, and the maximum normalized out-of-plane displacement along the member length $\Delta_{out\text{-}of\text{-}plane}/L$ is plotted against the member slenderness ratio L_b/r_y in Fig. 9b. The subduction interface ground motion yielded the largest values for both parameters.

Referring to Fig. 9a, axial shortening increased as a result of higher axial loads, which was confirmed by the past experimental studies (Elkady and Lignos 2018a). Moreover, the columns of MRF-D2 experienced the largest axial shortening (i.e., 1.1%L for interior and 0.6%L for exterior columns). Past full-scale experimental tests (Elkady and Lignos 2018b) showed that large out-of-plane deformations are expected near the base plastic hinge region when the column axial shortening exceeds 1%L. Such out-of-plane deformations can cause considerable weak-axis moments due to member P-Delta forces, in particular when the column experiences large drift demands. The current stability design requirements in CSA S16 neglect explicitly checking column axial shortening and instead attempt to control axial shortening by limiting the width-to-thickness and compressive axial load ratios, which both are more quantitative design parameters. Finally, the evaluation of the axial load demand for interior columns shows that the gravity-induced axial load of interior columns in a well-designed MRF is significantly lower than $0.30AF_y$, i.e., $0.09AF_y$, $0.16AF_y$, and $0.17AF_y$ in MRFs-S, D1 and D2. The axial load ratio can be higher (e.g., $0.40AF_y$) in existing MRFs (Bech et al. 2015).
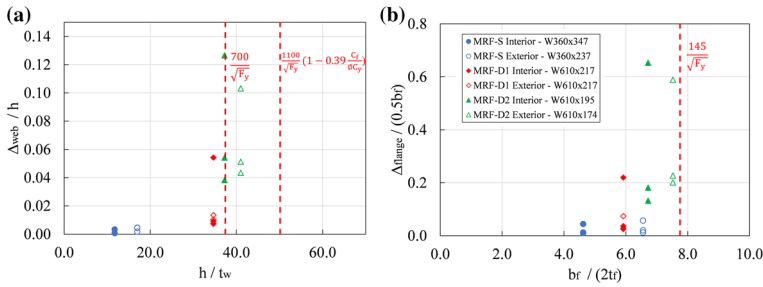
Fig. 10 **a** Normalized web out-of-plane displacement versus web slenderness ratio; **b** normalized flange out-of-plane displacement versus flange slenderness ratio

The most critical peak out-of-plane displacements was observed for the W610×195 column with an amplitude of 0.10%L (Fig. 9b). Although this column meets the axial load ratio of 0.30AF_y, the out-of-plane deformation combined with the observed axial shortening of 1.1%L suggest that the axial load limit alone may not be sufficient to limit axial shortening and subsequent strength degradation.

Referring to Fig. 9a, b, exterior columns of all three design scenarios always have smaller shortening and out-of-plane displacement compared to their interior counterparts. Although the axial load of exterior columns can reach and exceed the 0.30AF_y limit, they experienced lower axial shortening (e.g., < 1.0%L) due to the benefit of dynamic overturning effects, which reduces their axial compression load. This suggests that the axial load limit of 0.30AF_y can be relaxed for exterior columns.

5.4 Influence of section compactness

Web and flange out-of-plane deformations near the column base plastic hinge where local buckling develops were measured for the columns studied. Figure 10 shows the peak values of web and flange deformations normalized by the web clear depth h and half of the flange width 0.5b_f, respectively. As shown, the smallest amplitude was always observed for the columns of MRF-S. This is in part attributed to the role of lower section slenderness ratios in delaying local buckling, which is consistent with the observations of past experimental studies (Newell and Uang 2008). Although sections conforming to Class 2 web or flange were not investigated in this study, the trends observed in Fig. 10a, b suggest that the specified Class 1 limit for the flange, Class 1 limit for the web of the columns with an axial load ratio lower than 0.15AF_y, and 700/(F_y)$^{0.5}$ limit for the web of the columns with an axial load ratio exceeding 0.15AF_y are necessary to prevent severe local buckling at the plastic hinge region and in turn limit axial shortening. Referring to Fig. 10a, b, both interior and exterior columns of MRF-D2 showed the largest local buckling amplitudes. Notably, the web deformations observed in MRF-D2 columns with a web width-to-thickness ratio near the limit (i.e., 37.0), are more than two times those recorded for MRF-D1 under the same ground motion record.

The current CSA S16 width-to-thickness limit of 37.0 for the columns under an axial load ratio exceeding 0.15AF_y can be obtained using the relationship between axial shortening, cumulative plastic rotation demand θ_{pl}, axial load and web width-to-thickness ratio proposed by Elkady and Lignos (2018b):

Fig. 11 Web width-to-thickness ratio of the studied columns versus axial load ratio as compared to web width-to-thickness ratio limits
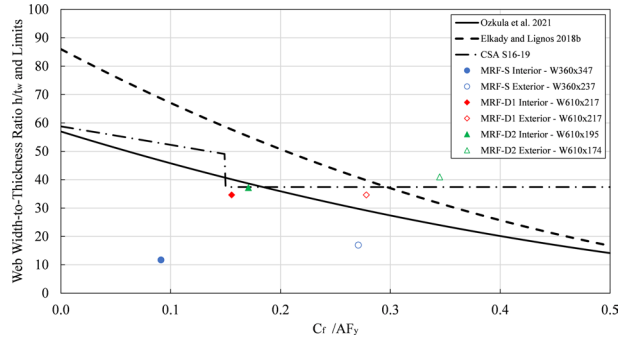
$$\Delta_{\text{axial}} = 13.62 \sum \theta_{\text{pl}}^{1.596} \left(\frac{h}{t_{\text{w}}}\right)^{0.769} \left(1 - \frac{C_{\text{f}}}{AF_{\text{y}}}\right)^{-1.819} \qquad (6)$$

where axial shortening Δ_{axial} is calculated in mm. The width-to-thickness limit $h/t_{\text{w}} = 37.0$ can be obtained for a column with an assumed unbraced length of 4600 mm and the axial load ratio of 0.30 by limiting axial shortening to $1\%L$ ($= 46$ mm) when the cumulative plastic rotation $\sum \theta_{pl}$ of 0.25 is attained.

Flexural strength degradation and local buckling amplitudes observed in this study for the W610×195 column of MRF-D2 reaffirms the need for a stricter width-to-thickness limit for first-story fixed-base columns in steel MRFs, similar to the one prescribed in the 2019 edition of CSA S16. This is consistent with a more stringent width-to-thickness ratio for the web proposed recently based on full-scale experimental testing of deep wide-flange columns (Ozkula et al. 2021):

$$\frac{h}{t_{\text{w}}} = 2.5\left(1 - C_{\text{a}}\right)^{2.3} \sqrt{\frac{E}{R_{\text{y}}F_{\text{y}}}} \qquad (7)$$

where C_{a} represents the column axial load ratio based on the expected axial capacity $AR_{\text{y}}F_{\text{y}}$. Using this equation, the web width-to-thickness ratio decreases as the member axial load increases.

Figure 11 compares the limits of Eqs. 6 and 7 with that of CSA S16 by varying the axial load ratio. The web slenderness limit of Class 1 sections is used for the axial load ratios below $0.15AF_{\text{y}}$ in this figure for CSA S16. The web width-to-thickness ratio of the first-story columns of the MRFs studied here are also shown at the maximum axial compression load observed under the 2011 Tohoku, Japan—YMT002 record. As shown in Fig. 11, the CSA S16 limit is less conservative when compared to the limit proposed by Ozkula et al. (2021), while Eq. 6 yields a more relaxed limit. This can be attributed to the fact that Eq. 7 does not explicitly account for the effect of axial shortening and takes a more conservative approach to account for boundary conditions, loading protocol and axial load history. Moreover, the CSA S16 limit beyond the axial load ratio equal to 0.3 is not applicable because the columns having an axial load ratio exceeding 0.3 are not permitted for the first-story columns by this standard.

6 Recommendations for improved seismic design

The stability design requirements prescribed by the Canadian steel design standard for columns of MRFs significantly improved the performance of deep wide-flange columns under the design level hazard representing a major seismic event with 2% probability of exceedance in 50 years. These requirements can, however be improved further based on the findings of this study.

The NLRHA results confirmed that the current CSA S16 lateral bracing limit of $L_b/r_y = 50$ appears to be highly conservative, and $\kappa = 0.45$ can be used in design, which results in $L_b/r_y = 70$. This new limit would permit more slender columns to be used in steel MRFs, creating a broader column selection for designers. Furthermore, the results obtained from CFEM analyses of deep columns exceeding the current lateral bracing limit support the proposed relaxation to this limit as neither member instability nor excessive out-of-plane deformation was present under design level earthquakes.

The current CSA S16 axial load limit of $0.30AF_y$ primarily influences the selection of exterior columns for which the axial load can approach or exceed this limit due to dynamic overturning effects. This limit can be increased to $0.35AF_y$ for the exterior columns as they are subjected to lower moments and varying axial load demands, making them less prone to severe strength degradation (e.g., $M_{rx} > 0.8R_yM_p$), axial shortening (e.g. $< 1.0\%L$) or member instability.

The limiting width-to-thickness ratio h/t_w of 37.0 for the web of wide-flange members in CSA S16 appears to be adequate at axial loads around $0.15AF_y$ based on CFEM analyses performed considering the effects of influential parameters including axial shortening cumulative plastic rotation demand and axial load.

Characterizing the stability response of steel MRF columns under cyclic displacement histories (e.g., Elkady and Lignos 2018a, b; Ozkula et al. 2017b, c) such as the symmetric cyclic loading protocol recommended by AISC Seismic Provisions (2016) or collapse-consistent loading protocols (Suzuki and Lignos 2020) may result in conservative demands in regions where near field earthquakes are expected, but such displacement histories can provide an envelope of anticipated seismic demands in regions with deep and long duration earthquakes such as subduction interface earthquakes expected in the west coast of Canada (Suzuki and Lignos 2021). Such standard loading protocols, however, ignore the influence of the rest of the structure on column demands and may not necessarily account for the ground motion characteristics specific to the building location. Thus, the loading histories based on a large set of ground motion records to characterize the response of steel MRF columns and examine seismic design requirements can supplement the findings from analyses and experiments performed using standard loading protocols.

7 Conclusions

This study aimed to critically evaluate the seismic design requirements for wide-flange steel columns part of Ductile (Type-D) MRFs with emphasis on the requirements prescribed by the Canadian steel design standard and propose improvements for enhanced stability design. Three design scenarios were considered: (1) square columns with $d/b_f \approx 1.0$ designed in accordance with the standard, (2) deep columns with $d/b_f \approx 1.9$ designed in accordance with the standard, and (3) deep columns with $d/b_f \approx 1.9$ designed excluding the stability design provisions specified in the standard for MRF columns. The seismic

response of the MRFs with the focus on their seismic design parameters was first evaluated using the NLRHA. The three-dimensional CFEM of the first-story interior and exterior columns part of the selected MRFs was then used to examine the limiting width-to-thickness ratio for the web, global slenderness and, axial load ratios, and propose improvements to these limits. The main findings of this study are summarized below:

- MRFs designed using deep wide-flange columns ($d/b_f \approx 1.9$) on average experienced lower lateral displacements than those designed using square columns. The reduction in story drift demands was greater than 10%. Additionally, utilizing deep wide-flange column sections in steel MRFs can reduce lateral load-resisting system weight by over 20%.

- The results obtained from the NLRHA suggest that the strong column-weak beam check at the beam-to-column joint may not be sufficient to prevent member instability and ensure elastic response of the columns above the first story. The verification of in-plane and out-of-plane stability of these columns under gravity loads and bending arising from beams reaching their probable flexural resistance is necessary.

- The evaluation of κ values using the NLRHA showed that, on average, $\kappa = 0.45$ can be used for first story columns, which results in a lateral bracing limit of $L_b/r_y = 70$. This finding supports the possibility of relaxing the L_b/r_y limit to a value much larger than the suggested limit of 50, provided that the column meets all the other prescribed strength and stability requirements by CSA S16.

- The deep W610×195 section, when used as the interior column of an MRF that violates the lateral bracing and web slenderness limits in the first story, and axial force–bending interaction check in the second story, collapsed under one of the ground motion records representing the design level hazard. This column exhibited flexural strength degradation of approximately $0.16R_yM_p$ at 6.5% chord rotation due to severe local buckling and out-of-plane deformations at the base plastic hinge. This observation confirmed the need for special seismic design provisions for columns in steel MRFs.

- The current CSA S16 axial load limit of $0.30AF_y$ for exterior first-story columns is conservative and can control the design of such columns. The limit for exterior first-story columns can be increased to $0.35AF_y$ as the exterior columns subjected to the proposed axial load limit in this study exhibited stable seismic response with the moment capacity always largely exceeding $0.80R_yM_p$ at large chord rotations exceeding 2.5%, and axial shortening well below 1.0%L. This is attributed to fluctuating axial loads that reach below the imposed gravity loads in compression due to the benefit of dynamic overturning effects. The axial load limit has a lesser effect on the selection of interior first-story columns because such columns are often subjected to gravity loads only, which are usually below this limit in a Type D steel MRF.

- The results of CFEM confirmed that the limiting width-to-thickness ratio for the web of the first-story columns $h/t_w = 37.0$ is adequate at an axial load of approximately $0.15AF_y$. The adequacy of the limit for columns under higher axial loads deserve much attention in future studies.

The findings presented in this paper should be used within the range of parameters considered here. In particular, only the hazard representing the design-level response spectra (2% probability of exceedance in 50 years) was used to examine the performance of steel MRFs and make recommendations to improve the seismic design of steel wide-flange columns. Future studies should also investigate the collapse performance of such frames. Moreover, the CFEM developed in this study neglects explicit modeling of the

beam-to-column web panel zone joint and the upper story columns. The influence of torque imposed by story beams and out-of-plane bending produced in the column due to plastic hinging of the base were not considered in the analyses performed here. Future studies should validate the analysis results presented in this study using hybrid simulation of steel MRFs or numerical modelling of beam-column subassemblies by explicitly simulating upper-story columns and beam-to-column web panel zone joints.

Availability of data and materials Not applicable.

Code availability Not applicable.

Declarations

Conflict of interest The authors declare they have no relevant financial or non-financial interests to disclose.

Consent to participate Not applicable.

Consent for publication Not applicable.

Ethical approval Not applicable.

References

AISC (2016a) ANSI/AISC 303-16, code of standard practice for steel buildings and bridges. American Institute of Steel Construction. Chicago, IL, USA

AISC (2016b) ANSI/AISC 341-16, seismic provisions for structural steel buildings. American Institute of Steel Construction. Chicago, IL, USA

Ashrafi A, Imanpour A (2021) Seismic response of steel multi-tiered eccentrically braced frames. J Constr Steel Res 181:106600

ASTM (2003) ASTM A6/A6M-04b, standard specification for general requirements for rolled structural steel bars, plates, shapes, and sheet piling. American Society for Testing and Materials, West Conshohocken

Bansal JP (1971) The lateral instability of continuous steel beams. University of Texas, Austin

Bech D, Tremayne B, Houston J (2015) Proposed changes to steel column evaluation criteria for existing buildings. In: Second ATC & SEI conf. on improving the seismic performance of existing buildings and other structures. American Society of Civil Engineers, San Francisco, CA

Bruneau M, Uang C-M, Sabelli R (2011) Ductile design of steel structures, 2nd edn. McGraw-Hill, New York

Canadian Standards Association (2019) CSA S16, Design of steel structures. CSA Group, Mississauga, ON, Canada

CISC (2014) Moment connections for seismic applications, 2nd edn. Canadian Institute of Steel Construction, Markham

Computer & Structures Inc (2019) SAP2000. Walnut Creek, CA, USA

Dassault Systemes Simulia Corp (2020) Abaqus-fea/cae. RI, USA

de Castro e Sousa A, Suzuki YA, Lignos D (2020) Consistency in solving the inverse problem of the voce-Chaboche constitutive model for plastic straining. ASCE J Eng Mech 146(9):04020097

Elkady A, Lignos D (2014) Analytical investigation of the cyclic behavior and plastic hinge formation in deep wide-flange steel beam-columns. Bull Earthq Eng 13(4):1097–1118

Elkady A, Lignos D (2017) Stability requirements of deep steel wide-flange columns under cyclic loading. In: Annual stability conference structural stability research council, Chicago, USA

Elkady A, Lignos D (2018a) Full-scale testing of deep wide-flange steel columns under multi axis cyclic loading: loading sequence, boundary effects, and lateral stability bracing force demands. ASCE J Struct Eng 144(2):04017189

Elkady A, Lignos D (2018b) Improved seismic design and nonlinear modeling recommendations for wide-flange steel columns. ASCE J Struct Eng 144(9):04018162

FEMA (2000a) Recommended seismic design criteria for new steel moment-frame buildings, FEMA-350. Federal Emergency Management Agency, Washington, DC, USA

FEMA (2000b) State of the art report on connection performance, FEMA-355D. Federal Emergency Management Agency, Washington, DC, USA

Galambos TV, Ketter RL (1958) Columns Under Combined Bending and Thrust. Fritz Engineering Laboratory Report 205A.21, Bethlehem, Pennsylvania

Gupta A, Krawinkler H (1999) Seismic demands for the performance evaluation of steel moment resisting frame structures. The John A. Blume Earthquake Engineering Center, Stanford University, Standford

Hartloper A, de Castro e Sousa A, Lignos D (2021) Constitutive modeling of structural steels: nonlinear isotropic/kinematic hardening material model and its calibration. ASCE J Struct Eng. https://doi.org/10.1061/(ASCE)ST.1943-541X.0002964

Imanpour A (2015) Seismic response and design of steel multi-tiered concentrically braced frames. Ph.D. Thesis. Polytechnique Montréal

Imanpour A, Lignos D, Clifton C, Tremblay R (2016) Comparison of seismic design requirements for steel moment resisting frames with emphasis on stability of columns in North America, New Zealand, and Europe. In: 11th pacific structural steel conference, Shanghai, China

Cravero J, Elkady A, Lignos D (2020) Experimental evaluation and numerical modeling of wide-flange steel columns subjected to constant and variable axial load coupled with lateral drift demands. ASCE J Struct Eng 146(3):04019222

Krawinkler H, Ibarra L (2005) Global collapse of frame structures under seismic excitations. The John A. Blume Earthquake Engineering Center, Stanford University, Standford

Lignos D, Krawinkler H (2011) Deterioration modeling of steel components in support of collapse prediction of steel moment frames under earthquake loading. ASCE J Struct Eng 137(11):1291–1302

Lignos D, Hartloper A, Elkady A, Deierlein G, Hamburger R (2019) Proposed updates to the ASCE 41 nonlinear modeling parameters for wide-flange steel columns in support of performance-based seismic engineering. ASCE J Struct Eng 145(9):04019083

MacRae GA (1990) The seismic response of steel frames. University of Canterbury Research Report 90-6, University of Canterbury, Christchurch, New Zealand

Nakashima M, Takanashi K, Kato H (1990) Test of steel beam-columns subject to sidesway. ASCE J Struct Eng 116(9):2516–2531

McKenna F, Fenves GL, Scott MH (1997) Open system for earthquake engineering simulation (OpenSees). University of California, Berkeley

National Research Council of Canada (2015) National building code of Canada 2015. Canada, Ottawa

Newell J, Uang C-M (2008) Cyclic behavior of steel wide-flange columns subjected to large drift. ASCE J Struct Eng 134(8):1334–1342

NRC-Commentaries (2015) User's Guide—NBC 2015 structural commentaries (Part 4 of Division B). Associate Committee on the National Building Code, Ottawa, ON

Ozkula G, Harris J, Uang C-M (2017a) Observations from cyclic tests on deep, wide-flange beam-columns. Eng J Am Inst Steel Constr 54:45–60

Ozkula G, John H, Uang C-M (2017b) Classifying cyclic buckling modes of steel wide-flange columns under cyclic loading. In: ASCE structures congress, pp 155–167

Ozkula G, Harris J, Uang C-M (2017c) Cyclic backbone curves for steel wide-flange columns: a numerical study. Ce/papers 1(2–3):3365–3374

Ozkula G, Uang C-M, Harris J (2021) Development of enhanced seismic compactness requirements for webs in wide-flange steel columns. ASCE J Struct Eng 147(7):04021100

Popov E, Chandramouli S (1975) Hysteretic behavior of steel columns. Earthquake Engineering Research Center, University of California, Berkeley

Popov E, Yang T, Chang S (1998) Design of steel MRF connections before and after 1994 northridge earthquake. Eng Struct 20(12):1030–1038

Ricles JM, Zhang X, Lu LW, Fisher J (2004) Development of seismic guidelines for deep-column steel moment connections. ATLSS Report No. 04-13, Lehigh University, Bethlehem, PA, USA

Shen J, Astaneh-Asl A, McCallen DB (2002) Use of deep columns in special steel moment frames. Steel Tips, Structural Steel Educational Council

Suzuki Y, Lignos DG (2020) Development of collapse-consistent loading protocols for experimental testing of steel columns. Earthq Eng Struct Dyn 49(2):114–131. https://doi.org/10.1002/eqe.3225

Suzuki Y, Lignos DG (2021) Experimental evaluation of steel columns under seismic hazard-consistent collapse loading protocols. J Struct Eng 147(4):04021020. https://doi.org/10.1061/(ASCE)ST.1943-541X.0002963

Tremblay R, Atkinson GM, Bouaanani N, Daneshvar P, Leger P, Koboevic S (2015) Selection and scaling of ground motion time histories for seismic analysis using NBCC 2015. In: The 11th Canadian conference on earthquake engineering, Vancouver, BC, Canada

Uang C, Ozkula G, Chansuk P (2019) Research on seismic design of deep wide-flange steel columns in the U.S. In: 12th Pacific structural steel conference, Tokyo, Japan

Zhang X, Ricles J (2006) Experimental evaluation of reduced beam section connections to deep columns. ASCE J Struct Eng 132(3):346–357

Yu QS, Gilton C, Uang C-M (2000) Cyclic response of RBS moment connections: loading sequence and lateral bracing effects. Rep. No. SSRP-99/13, Dept. of Structural Engineering, Univ. of California, San Diego, CA

Zareian F, Medina R (2010) A practical method for proper modeling of structural damping in inelastic plane structural systems. Comput Struct 88:45–53